CREEP AND HIGH TEMPERATURE LOW CYCLE FATIGUE OF

CAST Ti-6Al-2Sn-4Zr-2Mo ALLOY

Shahid Bashir and Malcolm C. Thomas

Materials and Processes Engineering, P.O. Box 420
Allison Gas Turbine Division, General Motors Corporation
Indianapolis, Indiana 46206-0420, U.S.A.

Abstract

Increasingly longer life requirements in the hot section of jet engines require reduced weight but still maintain high temperature capability. Large highly complex shaped structural components of jet engines like compressor case and diffuser offer significant weight and cost savings if made from titanium castings instead of the traditional high-strength steels or nickel-base superalloys. Cast Ti-6-2-4-2 alloy in the HIP and aged condition was analyzed for creep and high temperature low cycle fatigue for use up to about 783°K (950°F). The wide variability in the observed creep behavior, and in the high temperature low cycle fatigue properties is related to the microstructure and fracture behavior. A heat-treat modification is suggested to improve these properties by refining the microstructure.

Introduction

The increasingly demanding requirements of reduced weight and cost, and higher temperature creep and low cycle fatigue capability of components in modern aircraft jet engines are met either by developing new alloys or by improving the properties of existing alloys with modifications in chemistry, heat treatment or processing. Modification of existing alloys is substantially less costly than developing new alloys.

Due to lower density, titanium alloys are an attractive alternative to the heavier nickel-base superalloys and structural stainless steels provided they can meet the high temperature requirements of jet engines. For making large structural components like turbine cases and housings, near net shape forming technology e.g. casting and powder metallurgy (P/M) offer cost advantage over machined wrought products (1). Compared to forgings, however, castings are prone to internal porosity and the microstructure is generally more variable, mainly due to differences in solidification rates within the same part, and coarser since refinement by forging is absent. The resultant properties would therefore be lower and have larger scatter than similar wrought components. Although advances in investment casting and hot isostatic pressing (HIP'ing) have provided partial solutions to these problems, limited data and experience with titanium cast parts has led to the use of "casting factors" in the design of airframe and jet-engine components (2,3). This penalizes the weight benefits of titanium alloys. To gain fuller advantage of cast titanium alloys and help eliminate the use of casting factors, a better understanding of microstructure - property relationships becomes even more important (4).

Titanium '92
Science and Technology
Edited by F.H. Froes and I. Caplan
The Minerals, Metals & Materials Society, 1993

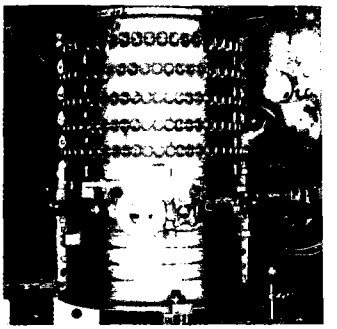

Figure 1. Compressor case of the Allison T406 engine.

Results And Discussion

Microstructure

Typical microstructures for the two fully heat treated conditions are shown in Figure 2. Condition A (Figures 2a and 2b) has numerous variants of alpha plates, the alpha colony size is irregular and the

a b c d

Figure 2. Microstructure of cast Ti-6242 for the two heat treatments; (a) and (b) fast cool, condition A, cooling rate @ 311°K (100°F)/min., (c) and (d) slow cool, condition B, cooling rate @ 270-275°K (25-40°F)/min.

grain boundary alpha is generally thick and continuous. Some areas consist of basketweave alpha. X-rays did not reveal any internal pores in the test pieces. The cooling rate from solution anneal temperature is about 311°K (100°F)/min (Ar gas fan cool at 0.4 MPa [60 psi]) and is termed as fast cool. The irregular structure of this condition is a result of the different section sizes and rapid cooling from the near beta solution anneal temperature, so that insufficient time is available for diffusion of alpha stabilizers. Although not studied here, the aging cycle is well understood to stabilize alpha.

For condition B, the alpha morphology is aligned acicular with very few remnants of basketweave structure (Figures 2c and 2d). The continuous grain boundary alpha and the alpha plates in the colonies appear finer than in condition A. Generally the colony size was more consistent but in some cases the alpha colony was as large as the prior beta grains. Again, no porosity was found. Furnace cooling with flowing Ar gas at 0.1 MPa (15 psi) gave a cooling rate of about 270-275°K (25-40°F)/min and is termed as slow-cool. The cast test bars had a consistent section size and more uniform structure. The slower cooling in condition B provided enough time for diffusion of alpha stabilizers and refined the alpha plates.

Tensile

Comparative tensile properties for the two conditions are summarized in Table III. Condition B maintained strength levels equivalent to the fast cooled condition A, but the ductility at both room temperature and at 755°K (900°F) is better. Better ductility in condition B is due to the fineness of the grain boundary alpha as well as the acicular alpha. This is similar to the ductility differences found

Table III. Average Tensile Properties for Conditions A and B

	Condition A		Condition B	
	RT	755°K (900°F)	RT	755°K (900°F)
UTS MPa (ksi)	965.3 (140)	606.7 (88)	972.2 (141)	655.0 (95)
0.2% YS MPa (ksi)	882.6 (128)	489.6 (71)	882.6 (128)	503.4 (73)
El (%)	8	13	17	19
RA (%)	10	23	22	40

in some alpha-beta alloys where the differences were attributed to the enlargement of microstructural unit and the grain boundary alpha (8). It is interesting to note, that in other alloys slower cooling rate had reduced ductility (9,10). However, the structures in these studies were bi-modal, i.e. acicular as well as equiaxed. In our case we only have the acicular phase. It can then be concluded that refinement of the acicular alpha morphology is beneficial in improving ductility.

Creep

Overall, creep resistance of condition B is remarkably better than condition A for the same test parameters (Figure 3). Time to reach 0.2% creep strain for the two conditions are compared in Table IV. For either condition no specimen failed before reaching 0.2% creep. In condition A, a creep-

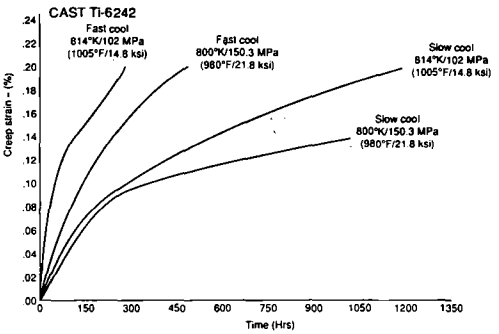

Figure 3. Comparison of creep behavior for conditions A and B at two stress/temperature conditions. Slow cool, condition B, is much more creep resistant.

Table IV. Comparison of 0.2% Creep

Test Parameters	Time to reach 0.2% creep (hr)	
	Cond. A	Cond. B
814°K/102 MPa (1005°F/14.8 ksi)	261	1217
800°K/150.3 MPa (980°F/21.8 ksi)	447	1022*

* test stopped after 1022 hr at 0.145% total creep strain.

ratchetting effect was observed during steady-state creep where the deformation occurred in small intermittent increments until it reached tertiary stage (Figure 4). This phenomenon was rarely present in condition B. The impressive difference in creep behavior can be rationalized in terms of the two microstructures.

For the integrally cast test bars (condition B), the alpha plate size within a colony is refined and the thickness of the grain boundary alpha is also reduced somewhat. Cooling rate, as discussed above, would not only affect the morphological changes but also the composition of alpha and other phases. Effects of different alpha morphologies obtained by different cooling rates in IMI 685 were shown to

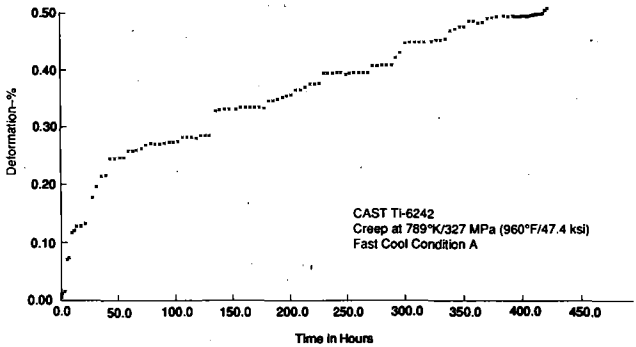

Figure 4. Creep-ratcheting seen in the fast cool, condition A, for a specimen tested at 788°K/326.8 MPa (960°F/47.4 ksi.)

have a minimum creep strain where the slower furnace cool (flowing Ar gas) gave the best creep properties as compared to the faster air cool or water quench rates (11). This was attributed, in part, to morphological changes. Similarly, in Ti-6242 (12) finer alpha platelet width improved creep resistance by restricting dislocation movement within alpha plates. The alpha-beta boundaries provided a sufficient barrier to substructure movement thus confining creep to alpha platelets. In effect, limiting of slip within alpha provided shorter mean path for deformation with the finer structure—similar to condition B in our case—hence better creep resistance. Coarser alpha platelets—condition A—would provide a larger area for dislocation movement and hence lower creep resistance.

One explanation for the ratchetting effect seen in condition A may be due to the large variability in the platelet size. When creep deformation concentrated within the alpha platelets, as discussed above, encounters a barrier to dislocation motion such as an alpha colony interface or coarse grain boundary alpha, detectable macro-creep would stop for a few hours till enough energy becomes available for overcoming the barrier, or for crossing over to a favorably oriented adjacent colony. At that instance a jump in creep strain is noticed. This also explains the larger scatter in creep observed for condition A. Uniformity of alpha morphology could explain the near absence of such steps in condition B.

A change in the apparent activation energy (slope of ln $\dot{\varepsilon}$ VS 1/T plot) indicates different operating creep mechanisms (13). In our study, the slope is essentially the same for the range of test temperatures (Figure 5), and it is therefore concluded that only one mechanism is dominant. Although

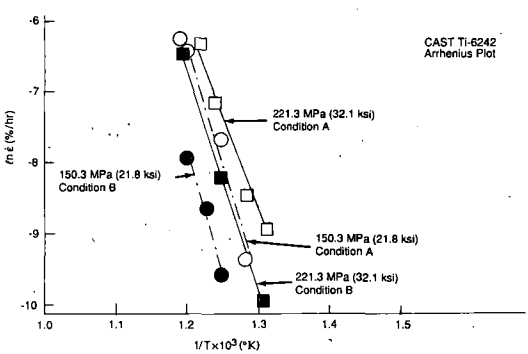

Figure 5. Arrhenius plot of conditions A and B at two stress levels.

the exact mechanism can only be characterized by transmission electron microscopy, following the above discussion, perhaps dislocation glide is the mechanism here.

Low Cycle Fatigue

The smooth bar LCF crack initiation life for condition B is better than condition A at 755°K (900°F) (Figure 6). The mean stress at half-life (Ni/2) is also higher (Figure 7), but better LCF life for condition B indicates that for the same 'R' ratio ($R_\varepsilon = 0$), the mean stress effects are more pronounced for condition A, or that condition B has better stress capability.

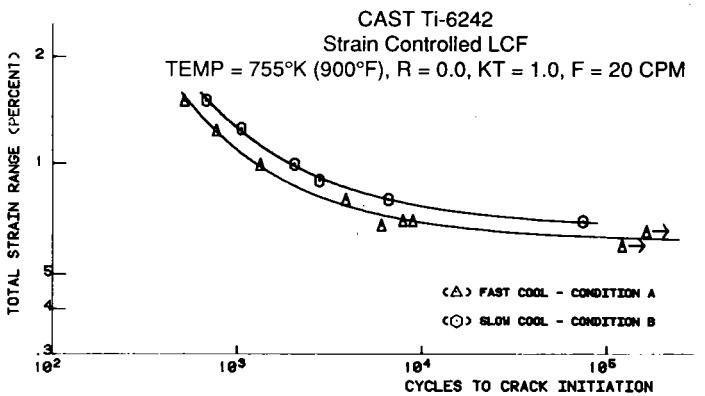

Figure 6. Comparison of smooth bar low cycle fatigue at 755°K (900°F) for conditions A and B.

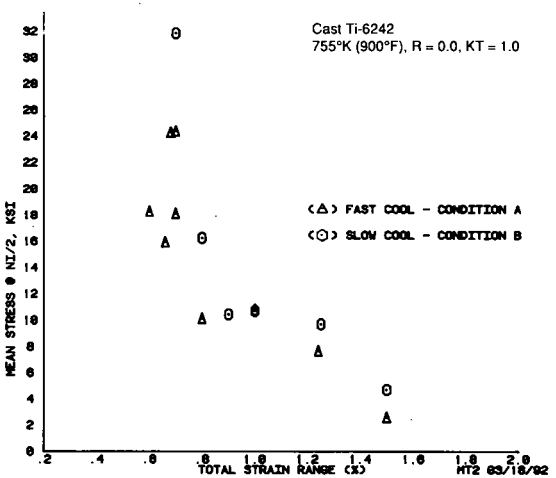

Figure 7. Cyclic mean stress at half-life ($N_i/2$). Despite higher mean stress, the LCF life of condition B was higher.

SEM fractography of condition A shows a crystallographic surface initiation and transition to Stage II mode. (Figure 8a). The cracks propagated by shearing at the interfaces of the alpha platelets, as is shown in Figure 8b. For condition B at the same total strain range (0.7%) the life increased by 7X. The origin is at a subsurface cluster of second phase particles (Figures 8c and 8d), probably equiaxed grain

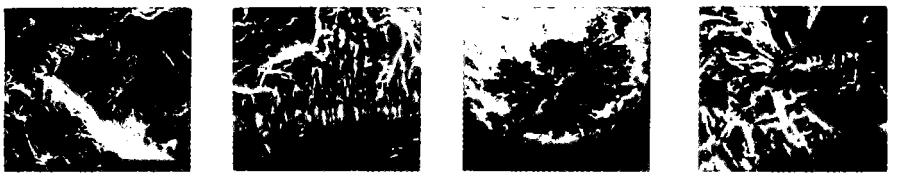

Figure 8. SEM fractographs of LCF specimens tested at total strain range of 0.7%; (a) surface crack initiation and (b) propagation along alpha platelets in condition A; (c) subsurface crack initiation and (d) high magnification of the origin which was at a cluster of second phase particles.

boundary alpha which was present at a few prior beta grain boundaries. Cracks also initiated at favorably oriented single colonies and propagated across the alpha plates by intense shearing. Note in Figure 9 that the cracking is almost at 90 deg to the platelets until it reaches the adjacent colony and changes direction, thereby increasing the tortuisity of the crack path.

Figure 9. Polished and etched longitudinal cross section of LCF specimen for condition B. This micrograph is from the same specimen as in Figure 8.

At higher total strain-ranges (1.0%), initiation and propagation for both conditions were identical, i.e. crystallographic surface initiation and propagation through the length of fatigued surface. The shear stresses were high enough for the fracture to occur by shear along the favorably oriented alpha platelets. Figure 10 is a typical SEM fractograph of this mode. The superior LCF life of condition B is a result of the finer, stronger alpha morphology as it provides resistance to cracking, whereas the weaker interfaces of the rapidly cooled coarse irregular alpha of condition A crack easily.

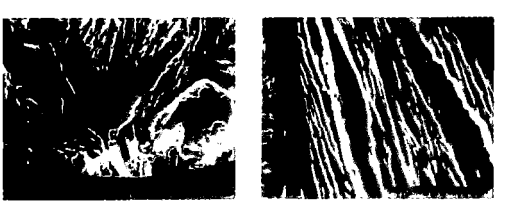

Figure 10. SEM fractograph of crystallographic crack initiation typical of both conditions A and B. This specimen was tested at 1.0% total strain range for condition B. (a) crack initiation and (b) propagation on crystallographic faces is by shear along the finer alpha platelets.

Most of the literature on microstructure-fatigue behavior of titanium alloys has concerned wrought alloys due mainly to use in fatigue critical components. Of the titanium alloys used in the cast form, only Ti-6Al-4V has been extensively studied. Consistent with our observations, Greenfield et. al. (14) noted that LCF initiation life was lower for the coarser alpha morphology, be it acicular or equiaxed.

Thus refinement of the alpha plates should improve LCF life. The equiaxed alpha-beta structure in wrought alloys is known to have better LCF life than the acicular alpha found in castings (15,16). Since an equiaxed alpha-beta structure is practically impossible to obtain in castings, and refinement of grain size in large structural castings is equally difficult, the optimum LCF capability in castings results from alpha refinement within the colonies as well as at the grain boundaries.

Conclusions

1. Improvement in creep of cast Ti-6242 alloy can be achieved without sacrificing LCF life or tensile ductility by suitably choosing heat treatment which refines acicular alpha and reduces continuous grain boundary alpha. A similar approach could possibly be applied to other cast titanium alloys.

2. Use of titanium castings in jet engines can be increased by improved understanding of microstructure-property relationships. Better understanding should help eliminate the use of "casting factors" which diminish the weight benefits of titanium alloys.

Acknowledgments

The authors wish to thank Allison Gas Turbine Division, General Motors Corporation, for permission to publish this paper. We acknowledge Precision Castparts Corporation (PCC), Portland, Oregon, for supplying the castings, M.A. Khan for testing, Ms. Marsha Gray for compiling the data, and Ms. Rita J. Wise for typing the manuscript.

References

1. B.A. Ewing, AGARD Conference Proceedings No. 325, 1982, pp. 13.1-13.12.
2. Military Specification, MIL-A-8860 (ASG), May 1960, para 3.2.1.1.
3. Federal Aviation Administration, DOT, Code of Federal Regulations, Title 14, Article 25.621. pp. 281-282.
4. D. Eylon, F.H. Froes, and R.W. Gardiner, *Titanium Technology – Present Status and Future Trends*, Edited by: F.H. Froes, D. Eylon and H.B. Bomberg, Titanium Development Association, 1985, pp. 35-47.
5. D. Eylon, S. Fujishiro, P.J. Postans, and F.H. Froes, in Reference 4, pp. 87-94.
6. S.R. Seagle and H.B. Bomberger, *The Science, Technology and Application of Titanium*, Edited by: R.I. Jaffee and N.E. Promisl, Pergamon Press, N.Y., 1970, pp. 1001-1008.
7. S.R. Seagle, G.S. Hall, and H.B. Bomberger, Met. Engr. Quarterly, Feb.1975, p. 48.
8. H.M. Flower, Mat. Sci. and Tech., Nov. 1990, vol. 6, pp. 1082-1092.
9. A. Vassel, F.H. Froes, J.P. Herteman and D. Eylon, Proc. Fifth International Conf. on Titanium, Munich, FRG, September 1984, pp. 515-521.
10. R.I. Jaffee, L. Wagner, and G. Lutjering, Proc. Sixth World Conf. on Titanium, Cannes, France, June 1988, pp. 1501-1506.
11. P.A. Blenkinsop, In Ref. 9, pp. 2323-2338.
12. W. Cho, J.W. Jones, J.E. Allison and W.T. Donlon, in Ref. 10, pp. 187-192.
13. P.J. Bania and J.A. Hall, in Ref. 9, pp. 2371-2378.
14. M.A. Greenfield, C.M. Pierce, and J.A. Hall, *Titanium Science and Technology*, Edited By: R.I. Jaffee and H.M. Burte, Plenum Press, N.Y. 1973, pp. 1731-1743.
15. N.D.R. Goddard, H.M. Flower, and M.J. Cope, In Reference 10, pp. 259-264
16. B. Vittemant and G. Thauvin; In Ref. 10, pp. 319-324.